ACTIVITY OF WATER IN THE DEEP EARTH, ORIGIN OF ABNORMAL PRESSURE, AND THEORY OF THERMO-OSMOTIC PRESSURE

Sergey Pivovarov
Institute of Experimental Mineralogy, Russian Academy of Sciences
142432 Chernogolovka, Moscow district, Russia
E-mail: serg@iem.ac.ru

Published on-line 22.12.2014

ABSTRACT

It is likely, that the deep Earth is specified by extra dry conditions, whereas the zones of abnormally high fluid pressure have local significance. One of possible causes for overpressuring is thermal diffusion of water. On theoretical grounds, this mechanism should be significant at low permeability, as the pore size decreases down to few nanometers, or the same, permeability decreases below ~ 10^{-20} m^2.

INTRODUCTION

ZONES OF ABNORMAL PRESSURE

Down to few kilometers, fluid pressure in the crust is close to hydrostatic profile (see **Fig. 1**):

$$P_{hyd}, \text{ bar} \sim 100\times[H, \text{ km}] + 1 \quad (1)$$

Here [H, km] is depth relative to surface (kilometers). Factor 100 bar/km corresponds to density of liquid 1.02 g/cm^3 (= 10/9.80665, where the denominator is acceleration of gravity). It should be noted that the real pressure in water column differs from Eq. (1) due to compressibility, thermal expansion, and salinity. Eq. (1) is just a nominal relation.

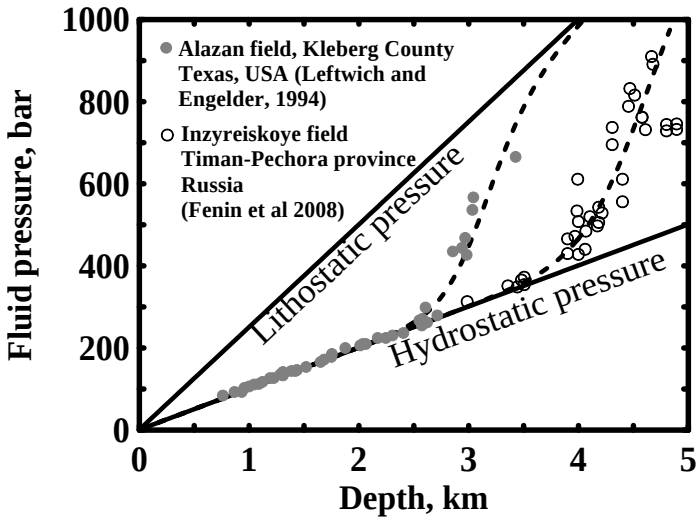

Fig. 1. Typical profiles of fluid pressure for oil fields. Solid circles: Alazan field, Kleberg County, Texas, USA, – data from Leftwich and Engelder (1994). Open symbols: Inzyreiskoye field, Timan-Pechora province, Russia – data from Fenin et al (2008). Solid lines: nominal hydrostatic and lithostatic pressures (Eqs. 1 and 2). Dashed curves are given for guidance.

At depths about few kilometers, fluid pressure often deviates from hydrostatic profile. Fluid pressure, larger or smaller than hydrostatic one, is called "abnormal pressure". In majority of cases, the abnormal pressure is larger than nominal hydrostatic one. As may be seen in **Fig. 1**, there are some reasons to suspect that the fluid pressure approaches with depth to lithostatic pressure:

$$P_{lit}, \text{ bar} \sim 250\times[H, \text{ km}] + 1 \quad (2)$$

Here factor 250 corresponds to density of rock 2.55 g/cm^3(practically, ranges from 2 to 3 g/cm^3).

If fluid pressure exceeds lithostatic one, it is not equilibrated with the weight of overlying rocks. This leads to fracturing (i.e., rising of hydraulic permeability) of overlying rocks and fast (and even explosive) discharge of the overpressured zone. Thus, at steady state, lithostatic profile is upper limit for fluid pressure.

During the drilling, fluid pressure at the bottom of well should be equilibrated with drilling fluid (frequently called as "mud"). In equilibrium, there is no outflow of drilling fluid, and no inflow of water into the well. Down to few kilometers, the efficient drilling fluid is water. In the zone of abnormally high pressure, the column of drilling fluid may be stabilized via dispersion of clays, barite, calcite, hematite (with small amounts of surfactants, in order to keep homogeneity of suspension). Knowing density of equilibrium drilling fluid (practically, up to 2.5 g/cm^3) and depth, one may calculate the fluid pressure at the bottom of well:

$$P_{fl}, \text{bar} \sim 10 \times g \times [\rho, \text{g/cm}^3] \times [H, \text{km}] + 1 \qquad (3)$$

Here g is acceleration (9.80665 N/kg = m/s^2), and [ρ, g/cm^3] is density (in g/cm^3). Data in **Fig. 1** were measured in this way (so called "mud weight method"). Each point corresponds to freshly excavated layer with relatively high hydraulic permeability (familiarly, "aquifer"). It should be also noted that the data in **Fig. 1** were collected from several wells in order to show regional trend (in both cases, number of wells was not specified).

Abnormally high pressures were detected in majority of oil and gas fields (Fertl, 1976; Hao et al, 2007; Fenin, 2010), and the data shown in **Fig. 1** are typical. Because of this, there is feeling, that below 4-8 km, there is global zone, where the fluid pressure is equal to lithostatic pressure. However this is not true.

FUGACITY AND ACTIVITY OF WATER

In **Fig. 2**, "petrologic" activity of water is shown as function of depth. The values of pressure and activity of water were calculated by Aranovich (1991) from chemical analyzes taken from published studies (data from Russia, Europe, Turkey, USA, Antarctica; pressure was converted into depth via Eq. 2). Each point corresponds to chemical analysis of coexisting minerals in the metamorphic rock, originated from large depth. Note that the values of pressure and activity of water were actual about few milliards of years ago (i.e., at origin). Now all these rocks are exposed to surface due to erosion. Nevertheless, minerals still remember their birthday.

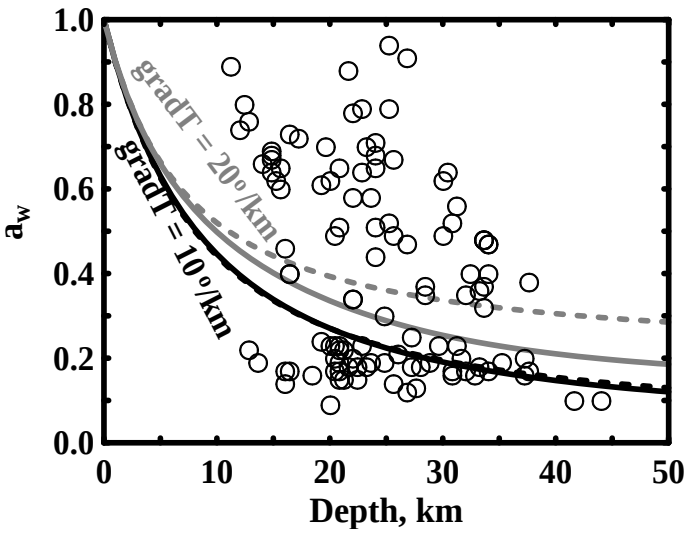

Fig. 2. "Petrologic" activity of water for variety of metamorphic complexes at origin (i.e., few milliards years ago). Data from Aranovich (1991; in original, values of pressure were given; depth was calculated from Eq. 2). Curves: hydrostatic equilibrium (see Eq. 5). Black curves: thermal gradient 10°/km. Gray curves: thermal gradient 20°/km. Solid curves: exact solution (Eqs. 5-13). Dashed curves: approximate solution (Eq. 17).

If pressure of aqueous fluid is equal to lithostatic pressure, activity of water should be close to 1. However, in spite of huge scatter of data in **Fig. 2**, the general trend is evident: activity of water decreases with depth. Thus, pressure of water in the deep Earth is much smaller than lithostatic pressure.

High activity of water (up to unit) may be generated due to dehydration of oceanic crust in the subduction zones. High activity of water leads to melting of rocks and formation of

volcanoes. In general case, volcanoes indicate high activity of water at large depth. And vise versa, the stable "lower crust" should be dry (Yardley and Valley, 1997). Volcanoes are not too abundant in the World, and thus, in global sense, the extra dry conditions should be typical for the deep Earth.

The "petrologic" activity of water may be defined as:

$$a_w = f_{act}/f_{lit} \quad (4)$$

Here f_{act} is actual fugacity of water (as calculated from mineral equilibrium), and f_{lit} is fugacity of pure water at given T and $P = P_{lit}$.

At least, down to few kilometers (see **Fig. 1**), low fluid pressure in pores and fractures is supported by hardness of grains. If pressure of water is defined as hydrostatic equilibrium of water column, the "petrologic" activity of water may be calculated as:

$$a_{w,\,hyd} = f_{hyd}/f_{lit} \quad (5)$$

Here f_{hyd} and f_{lit} are values of fugacity of pure water at given T and $P = P_{hyd}$ or P_{lit}.

The solid curves in **Fig. 2** were calculated from Eq. (5), applying P_{hyd} from Eq. (1), P_{lit} from Eq. (2), and T = 298 + 10×[H, km] or 298 + 20×[H, km]. The values of fugacity at given (T, P) were calculated from equation of state for pure water substance (Pivovarov, 2013):

$$f,\ bar = R_c \times T \times c \times Y \quad (6)$$

$$\ln(Y) = 2Ac - B\ln(1+\beta c)/\beta - Bc/(1+\beta c) - 1.5Cc^2[1-\exp\{-(Ac)^2\}] - Cc^4A^2\exp\{-(Ac)^2\} + (4/3)Dc^3 \quad (7)$$

$$P,\ bar = R_cT \times c\{1 + Ac - Bc/(1+\beta c) - Cc^2\{1 - (1 - (Ac)^2)\exp(-(Ac)^2)\} + Dc^3\} \quad (8)$$

Here R_c is "molarity-based" gas constant (as 0.0831441 $dm^3 \times bar \times mol^{-1} \times K^{-1}$), T is absolute temperature (K), c is molarity of water (moles per dm^3), Y is "absolute activity coefficient", A, B, β, C, D are model parameters (below q = 298.15/T):

$$A = 0.022699 + 0.0049722q/(1+0.539q^{12}) \quad (9)$$
$$B = 1.0629q \times \exp\{2.768(q-1)\} \quad (10)$$
$$\beta = 0.060225q^{1.9} + 0.20051q^{3.5} + 0.0035436q^{14} \quad (11)$$
$$C = 0.017461q^{2.9}/(1+6.701q^{2.3}) + 0.0016763q^{2.4}/(1+1.993q^{8.3}) \quad (12)$$
$$D = 0.000057006q + 0.000022393q/(1+1.54q^{9}) \quad (13)$$

In **Tab. 1**, the values of fugacity (bar) are given, as calculated from Eqs (6-13). The relations between molar volume, V_w, molarity, c, and density, ρ_w, are obvious:

$$V_w,\ cm^3/mol = 1000/[c,\ mol/dm^3] = [M_w,\ g/mol]/[\rho_w,\ g/cm^3] \quad (14)$$

$$\rho_w,\ g/cm^3 = [M_w,\ g/mol] \times [c,\ mol/dm^3]/1000 = [M_w,\ g/mol]/[V,\ cm^3/mol] \quad (15)$$

Here M_w = 18.0152 g/mol is molar weight of water. In **Tab. 2**, the values of density of water are given, as calculated from Eqs. (8-13, 15).

The values of "petrologic" activity of water in equilibrium with the hydrostatic column, as defined by Eq. (5), may be also calculated from:

$$\ln(f_{hyd}/f_{lit}) = -\int_{P_{hyd}}^{P_{lit}} V_w dP/RT \qquad (16)$$

Here P_{hyd} and P_{lit} are values of hydrostatic and lithostatic pressure (in Pa), V_w is molar volume of water (in m^3/mol), R is gas constant (as 8.3144 $J\times mol^{-1}\times K^{-1}$), and T is absolute temperature (K).

Volume changes for condensed substances are small, and Eq. (16) may be simplified to

$$\ln(f_{hyd}/f_{lit}) \approx -(P_{lit}-P_{hyd})V_w/RT = -[P_{lit}-P_{hyd}\text{ , bar}]\times[V_w\text{ , cm}^3\text{/mol}]/\{83.144\times T\} \qquad (17)$$

The dashed curves in **Fig. 2** were calculated with use of Eq. (17), assuming V_w = 18.07 cm^3/mol. At the thermal gradient 10°/km, exact solution (solid curves) coincides with approximate solution (dashed curves, Eq. 17). This is because the thermal expansion of water in column is compensated by compressibility, and density remains constant. Contrarily, at thermal gradient 20°/km, density of water decreases with depth. As may be seen in **Fig. 2**, activity of water in the deep Earth is generally consistent with hydrostatic equilibrium of water column.

Tab. 1 Fugacity of liquid water f_w (calculated from Eqs. 6-13). Sign "*" indicates supercooled liquid (in the field of ice). Bold italic style: low density gas-like state (in supercritical region).

T°C	f_w , bar							
	P_{sat}	100bar	200bar	500bar	1 kbar	2 kbar	5 kbar	10kbar
0	0.00612*	0.00662	0.00716	0.00905	0.0133	0.0280	0.2338	6.222*
25	0.0316	0.0340	0.0365	0.0453	0.0644	0.1282	0.9089	18.90*
50	0.1231	0.1317	0.1409	0.1722	0.2392	0.4544	2.824	47.96
100	0.9952	1.057	1.122	1.342	1.798	3.179	16.06	197.0
150	4.551	4.799	5.072	5.978	7.817	13.14	57.07	547.0
200	14.16	14.81	15.61	18.22	23.43	38.02	147.3	1166
250	33.77	34.84	36.67	42.59	54.19	85.70	304.2	2068
300	66.72	67.22	70.81	82.14	104.1	161.8	536.5	3222
400	-	***86.80***	***148.1***	203.7	261.4	401.8	1216	6078
600	-	***95.35***	***181.7***	***392.4***	637.5	1058	3007	12064

Tab. 2 Density of liquid water (calculated from Eqs. 8-13, 15). Sign "*" indicates supercooled liquid (in the field of ice). Bold italic style: low density gas-like state (in supercritical region).

T°C	ρ_w , g/cm^3							
	P_{sat}	100 bar	200 bar	500 bar	1 kbar	2 kbar	5 kbar	10 kbar
0	1.000*	1.005	1.010	1.024	1.044	1.080	1.160	1.253*
25	0.997	1.002	1.006	1.019	1.039	1.073	1.150	1.241*
50	0.988	0.992	0.997	1.009	1.028	1.061	1.137	1.226
100	0.959	0.963	0.968	0.981	1.001	1.035	1.112	1.201
150	0.916	0.922	0.927	0.943	0.966	1.003	1.085	1.176
200	0.863	0.869	0.877	0.896	0.924	0.967	1.056	1.152
250	0.798	0.805	0.815	0.842	0.877	0.928	1.027	1.129
300	0.715	0.718	0.736	0.777	0.824	0.887	0.997	1.105
400	-	***0.038***	***0.098***	0.580	0.694	0.794	0.935	1.057
600	-	***0.026***	***0.055***	***0.164***	0.371	0.588	0.809	0.964

PECULIARITIES OF SYSTEMS WITH UNEQUAL PRESSURE

Quasi-equilibrium between the fluid under hydrostatic pressure and solid rock under lithostatic pressure leads to some interesting phenomena. As may be seen in Eq. (17), the pressure jump on solid-water interface generates the jump in activity of water. This is true for any other condensed substance:

$$\Delta \ln(a) \approx - \Delta P V_m / RT = - [\Delta P \text{ , bar}] \times [V_m \text{ , cm}^3/\text{mol}] / \{83.144 \times T\} \quad (18)$$

Here a is "chemical reactivity" of substance (arbitrary units), V_m is molar volume of substance.

Fig. 3 shows the saturation index for quartz (compressed under lithostatic pressure) in pore fluid at hydrostatic pressure. Note that change in "reactivity" has the same sign for any substance and it is opposite to pressure change. For instance, at depth 3 km and t = 55°C, "reactivity" of water changes from 1 in liquid down to 0.74 (= f_{hyd}/f_{lit}) in solid. Similarly, for quartz (V_m = 22.7 cm^3/g): from 1.45 in liquid down to 1 in solid.

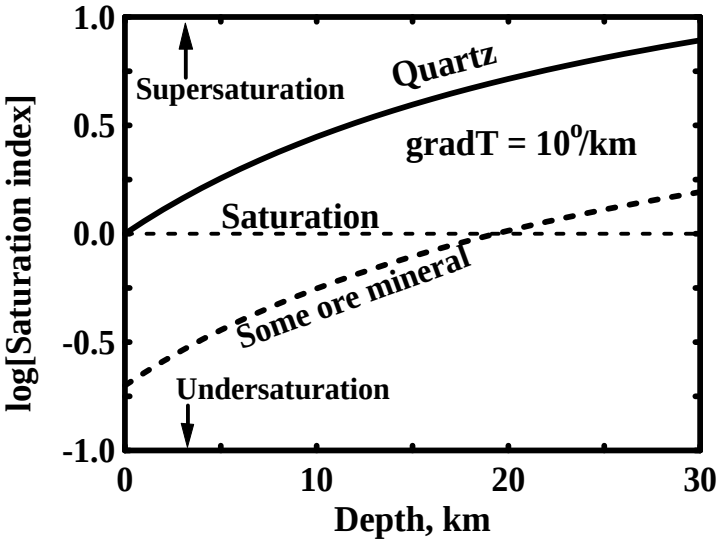

Fig. 3. Supersaturation of fluid at hydrostatic pressure in contact with quartz-bearing rock, compressed under litostatic pressure. "Some ore mineral" is the same curve, shifted by 0.7 log units.

In quartz-bearing rock, activity of quartz is unit by definition. However, in contact with decompressed fluid, quartz dissolves much better than at equilibrated pressure. Decompressed water in contact with compressed quartz becomes supersaturated, and this leads to recrystallization. However, time scale is highly dependent on temperature and pressure. Perhaps, at depth 3 km, healing of fractures takes thousands or millions of years and followed by growth of large transparent crystals. At depth 30 km, healing of fracture takes, perhaps, hours or months, and followed by growth of "milky" quartz and by "sub-melting" of rocks.

"Reactivity" of water in rock, equilibrated with hydrostatic column, is smaller than unit (see curves in **Fig. 2**). This means that, just below the Earth's surface, liquid water is unstable phase. Because of this, it is likely that, below ~ 30 km, fluid is temporal phase. Upon earthquake, newly opened fracture is first filled by vacuum. Then the fracture is occupied by volatile components (permanently adsorbed on grain interfaces and dissolved in minerals). Upon healing of fracture, fluid phase disappears. Similar temporal fluid phases may arise between the grains due to tectonic stress. Such intergranular lubricant serves the plastic flow in rocks (and glaciers as well).

If activity of mineral in rock is smaller than unit (e.g., a = $10^{-0.7}$ = 0.2, as for "some ore mineral" in **Fig. 3**), such mineral is absent in rock, although its chemical components present as admixtures to other minerals. However, extractive ability of fluid is strongly enhanced by decompression. At some depth, decompressed fluid may be supersaturated with respect to such mineral (see **Fig. 3**). Because of this, healing of fractures may be followed by crystallization of minerals, which are absent in parent rocks. Upon healing of fractures, such minerals become unstable due to compression back to lithostatic pressure. However, low permeability of rocks inhibits dissolution. Perhaps, fracturing and healing – upon each earthquake and during millions of years – is one of mechanisms for the formation of ores.

HYDRAULIC PRESSURE AND HYDRAULIC FLUX

If water column is compressed under lithostatic pressure, it is not equilibrated by its own weight. In such water column, the hydraulic pressure gradient is grad{P_h} = grad{P_{lit}} – grad{P_{hyd}} = 250 – 100 = 150 bar/km = 15000 Pa/m. More other, as may be seen in **Fig. 1**, the gradient of fluid pressure in the intermediate zone is about 500 bar/km, and thus, hydraulic pressure gradient is grad{P_h} = 500 – 100 = 400 bar/km = 40000 Pa/m. Thus, under the influence of hydraulic pressure gradient, water should flow to the surface.

Flux of water through the porous membrane is defined by Darcy law:

$$J, m/s = – K \times grad(P_h^*) \quad (19)$$

Here J is flux (m^3 of fluid per second, passed through the porous membrane with cross-section 1 m^2), K is conditional permeability (m/s), and grad(P_h*) is hydraulic pressure gradient, expressed in dimensionless units (e.g., cm of water column per cm of membrane). Sign minus means that flux J and hydraulic pressure gradient grad{P_h*} are directed in opposite.

The Darcy-Nutting equation is more convenient:

$$J, m/s = – \{k/\eta\} \times grad(P_h) \quad (20)$$

Here k is intrinsic permeability (m^2), η is dynamic viscosity of fluid (Pa×s), grad{P_h} is hydraulic pressure gradient (Pa/m). The values of viscosity η for liquid water are given in **Tab 3.** Relation between the intrinsic (k) and conditional (K) permeability is (numerical relation is valid for liquid water at 25°C and 1 bar):

$$k, m^2 = \{\eta/(\rho \times g)\} \times K = 9.11 \times 10^{-8} \times [K, m/s] \quad (21)$$

Here ρ is density of fluid (in kg/m^3), g is acceleration, 9.80665 N/kg or m/s^2. Intrinsic permeability is often expressed also in "Darcy" units:

$$k, m^2 = (1/1.01325) \times 10^{-12} \times [k, Darcy] \quad (22)$$

Here 1.01325 is atmosphere-to-bar conversion factor.

As measured by Yang and Aplin (2007) intrinsic permeability of "natural mudstones" in vertical direction is 2.4×10^{-22} – 1.6×10^{-19} m^2 (23 samples with clay content 12-66 %; by 1-2 samples from 16 wells: North Sea, Bay of Mexico; depth 2-5 km). Thus, at hydraulic pressure gradient ~ 400 bar/km = 40000 Pa/m (see **Fig. 1**) and viscosity η = 0.2952×10^{-3} Pa×s (at 100°C and 500 bar, see **Tab. 3**) the water flux to surface is 1-684 m of water column per million of years. This is senseless, if it has global significance.

Tab. 3 Pressure of saturated water vapor, and viscosity of liquid water (Grigull et al 1990).

T°C	P_{sat}, bar	η, 10^{-3} Pa×s			
		P_{sat}	100 bar	500 bar	1 kbar
0°C	0.0061*	1.793*	1.768	1.697	1.652
25°C	0.0317	0.8905	0.8884	0.8849	0.8901
50°C	0.1234	0.5471	0.5489	0.5574	0.5708
100°C	1.0130	0.2819	0.2845	0.2952	0.3084
150°C	4.757	0.1825	0.1849	0.1946	0.2060
200°C	15.536	0.1344	0.1365	0.1457	0.1560
250°C	39.736	0.1062	0.1078	0.1175	0.1275
300°C	85.838	0.08596	0.08652	0.09853	0.1091

Sign "*" indicates supercooled liquid (in the field of ice).

Average hydraulic flow velocity of water in straight flat channel is (Kutepov et al, 1996):

$$\upsilon_h = -\{h^2/12\eta\}\{\Delta P_h/\Delta L\} \quad (23)$$

Here h is thickness of flat channel, ΔL is total length of channel, ΔP_h is pressure difference between input and output of channel. If channel is curved on zig-zag manner, Eq (23) is:

$$\upsilon_{h,x} = \upsilon_h/\tau = -\{h^2/12\eta\tau^2\}\{\Delta P_h/\Delta X\} = -\{h^2/12\eta\tau^2\}\mathrm{grad}(P_h) \quad (24)$$

Here $\upsilon_{h,x}$ is penetration velocity, i.e., projection of actual flow velocity in zig-zag channel (υ_h) onto general direction of flow, τ is tortuosity (constant factor, about 1.5), $\Delta X = \Delta L/\tau$ is projection of the zig-zag flowpath onto general direction of flow.

Relation between the penetration velocity of water and flux is obvious:

$$J = \theta\times\upsilon_x \quad (25)$$

Here θ is porosity, and υ_x is overall penetration velocity (down to $k \sim 10^{-20}$ m^2, $\upsilon_x \approx \upsilon_{h,x}$). Thus, from Eqs (20, 24, 25), permeability of rock is defined by

$$k_h = \{\theta/12\tau^2\}\times h^2 \quad (26)$$

Here k_h is hydraulic permeability (down to $k \sim 10^{-20}$ m^2, $k_h \approx k$).

The average thickness of channel (fracture) in rock, or average distance between the particles in clay or sand, may be found from obvious relation:

$$h, m \sim 2\times10^{-3}/\{[S, m^2/g][Load, g/L]\} \quad (27)$$

Here [S, m^2/g] is specific surface area of solid, and [Load, g/L] is solid load (in grams per liter of fluid):

$$Load, g/L = 1000\times(1-\theta)\times[\rho_s, g/cm^3]/\theta \approx 1000\times(1-w)/w \quad (28)$$

Here θ is porosity (volume fraction), ρ_s is density of solid, w is weight fraction of water in rock.

From Eqs (26-28), one may obtain Kozeny-Carman equation (Carman 1937):

$$k_h, m^2 \sim \{C_g/(\rho_s S)^2\}\times\theta^3/(1-\theta)^2 = 10^{-12}\times\{C_g/([\rho_s, g/cm^3][S, m^2/g])^2\}\times\theta^3/(1-\theta)^2 \quad (29)$$

Here C_g is geometric constant, dependent on shape of porous medium. As estimated by Carman (1937) from experimental data, $C_g \approx 1/5 = 0.2$. From Eqs (26-29), applying $\tau = 1.5$:

$$C_g = \{2^2/12\tau^2\} \approx 0.15 \quad (30)$$

Specific surface area for uniform sand may be estimated from grain size:

$$S, m^2/g \approx 6\times10^{-3}/\{\rho_s d\} = 6\times10^{-3}/\{[\rho_s, g/cm^3]\times[d, mm]\} \quad (31)$$

Here d is diameter of spherical particle or side of cube. For uniform spherical or cubic particles, Eq. (31) is exact relation. With Eq. (31), Eq. (29) may be rewritten as (Carman, 1937):

$$k_h, m^2 \sim \{C_g/36\}\times d^2\times\theta^3/(1-\theta)^2 = 10^{-6}\times\{C_g/36\}\times[d, mm]^2\times\theta^3/(1-\theta)^2 \quad (32)$$

In **Figs. 4 and 5**, the Kozeny-Carman equation (Eqs. 29 and 32) is compared with experimental data from Djéran-Maigre et al (1998) and Beard and Weyl (1973). As may be seen, although the geometry of space between the particles is rather different from "flat channel", Kozeny-Carman equation works, at least, approximately.

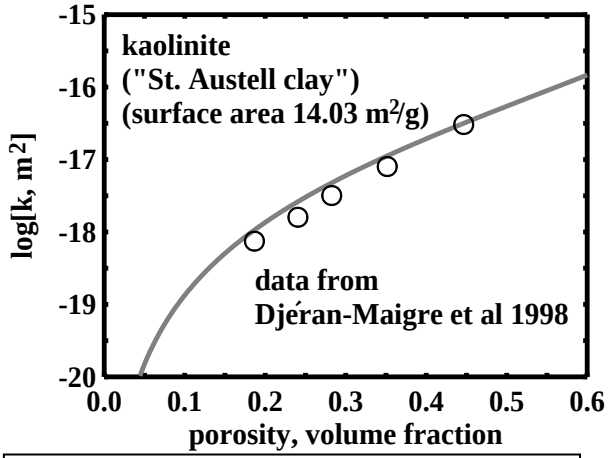

Fig. 4. Permeability of compacted kaolinite ("St. Austell clay"). Data from Djéran-Maigre et al (1998). Curve: Eq (29) with $C_g = 0.15$, $\rho_s = 2.65$ g/cm^3 and $S = 14.03$ m^2/g.

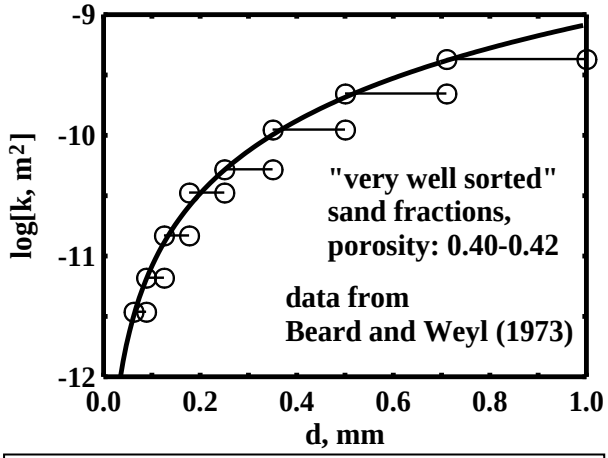

Fig. 5. Permeability of sieved fractions of sand (smallest and largest grain size in each fraction are connected with line). Data from Beard and Weyl (1973). Curve: Eq (32) with $C_g = 0.15$ and $\theta = 0.41$.

DIFFUSION

In addition to hydraulic flux, there is also diffuse flux, which appears to be significant at low permeability. From Fick's law, flux of dissolved substance may be written as:

$$\upsilon_d \text{ , m/s} = -D_c \times \{d\ln(c)/dx\} \qquad (33)$$

Here υ_d is average velocity of translation movement for molecule due to diffusion, D_c is c-dependent diffusion coefficient (m^2/s), c is concentration (e.g., moles per liter), x is distance (meters). The dependence of D_c on c is approximately consistent with Nernst-Hartley equation:

$$D_c = D^o \times \{1 + d\ln(\gamma)/d\ln(c)\} \qquad (34)$$

Here γ is activity coefficient, D^o is diffusion coefficient, which is less variable than D_c (but still not a constant). With Nernst-Hartley equation, Eq. (33) is

$$\upsilon_d \text{ , m/s} = -D^o \times \{d\ln(\gamma c)/dx\} \qquad (35)$$

At constant temperature, equality $d\ln(\gamma c) = d\ln(f)$ is exact relation, and Eq. (35) may be rewritten as:

$$\upsilon_d \text{ , m/s} = -D^o \times \{d\ln(f)/dx\} \qquad (36)$$

Diffusion coefficient D^o may be calculated from Stokes-Einstein equation**:**

$$D^o, \text{ m}^2/\text{s} = k_B T/\{6 \times \pi \times \eta \times r_h\} \qquad (37)$$

Here k_B is Boltzmann constant (1.380662e-23 J/K), T is absolute temperature (K), $\pi = 3.14159..$,

η is viscosity of medium (Pa×s; see **Tab. 3**), and r_h is "hydrodynamic radius" of particle, molecule, or ion. From value $D^o = 2.30\times10^{-9}$ m^2/s (Krynicki et al, 1978) for liquid water at 25°C and 1 bar, the hydrodynamic radius of water molecule r_h is 1.0663×10^{-10} m = 1.0663 Å.

In **Fig. 6** the Stokes-Einstein equation (Eq. 37) is compared with experimental self diffusion coefficient of water (Krynicki et al 1980). Curves were calculated with r_h = 1.0663 Å and viscosity η from **Tab 3**. It should be noted that the factor 6 in Eq. (37) stands for "hydrophilic spherical solid particles". For the case of, e.g., air bubble in water, it should be replaced by the factor 4. With factor 4 instead of 6, Eq. (37) gives r_h = 1.6 Å, which seems to be more realistic, than r_h = 1.0663 Å. However, the "hydrodynamic radius" of molecule is operational parameter. Thus, there is no significant sense in choice of "true factor". In spite of vague sense of "hydrodynamic radius" for a molecule, Stokes-Einstein equation gives surprisingly close agreement with experiment.

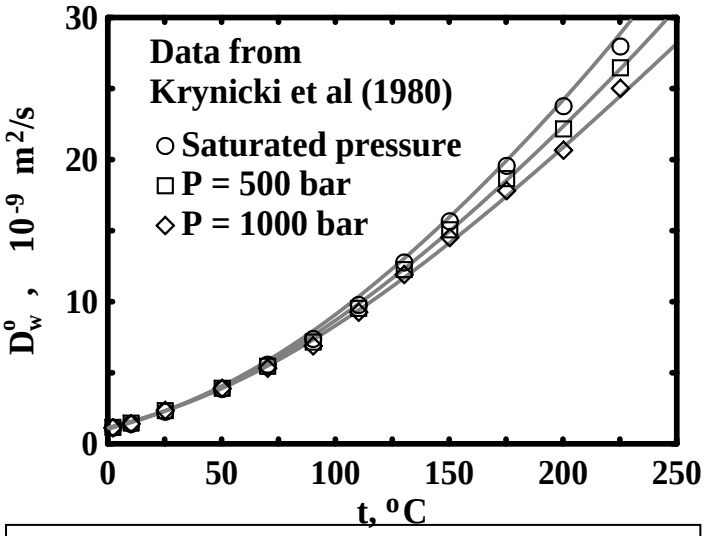

Fig. 6. Self diffusion coefficient of liquid water. Data from Krynicki et al (1980). Solid curves were calculated in accordance with Stokes-Einstein equation (Eq. 37), hydrodynamic radius of water molecule r_h = 1.0663 Å and viscosity from **Tab. 3**.

From general thermodynamics (Karapetyants, 1975):

$$\{\partial\ln(f)/\partial P\}_T\ ,\ Pa^{-1} = V_w/RT \qquad (38)$$

Here V_w is molar volume of water (in m^3/mol), and R is gas constant (as 8.3144 $J\times mol^{-1}\times K^{-1}$). From Eqs. (36, 38), pressure-driven diffuse velocity of water molecules in straight channel is

$$\upsilon_d\ ,\ m/s = -D^o\times\{V_w/RT\}\times\{\Delta P_h/\Delta L\} \qquad (39)$$

Here ΔP_h is pressure difference between input and output of channel, and ΔL is length of channel. If channel is curved on zig-zag manner, Eq. (39) is:

$$\upsilon_{d,x}\ ,\ m/s = \upsilon_d/\tau = -\{D^o/\tau^2\}\times\{V_w/RT\}\times\Delta P_h/\Delta X = -\{D^o/\tau^2\}\times\{V_w/RT\}\times grad(P_h) \qquad (40)$$

Here τ is tortuosity of channel (~ 1.5), $\Delta X = \Delta L/\tau$ is projection of the zig-zag flow path on general direction of flow. Taking D^o from Stokes-Einstein equation (Eq. 37), one may obtain:

$$\upsilon_{d,x}\ ,\ m/s = \{\sigma/\eta\}\times grad(P_h) \qquad (41)$$

$$\sigma\ ,\ m^2 = M_w/(6\times\pi\times N_A\times\rho_w\times r_h\times\tau^2) = 1.488\times10^{-20}/\{\tau^2\times[\rho_w\ ,\ g/cm^3]\} \approx 0.663\times10^{-20}/[\rho_w\ ,\ g/cm^3] \qquad (42)$$

Assuming $\upsilon_x = \upsilon_{h,x} + \upsilon_{d,x}$, one may obtain for overall permeability (see Eqs. 20, 24, 25):

$$k = k_h + \theta\times\sigma \qquad (43)$$

Here k_h is hydraulic permeability (see Eqs. 26, 29, 32).

ORIGIN OF ABNORMAL PRESSURE

Most popular idea is that the abnormally high pressure arises due to compression of sedimentary rocks, followed by contraction of the pore space. At low permeability, this leads to partial capture of fluid in pore space and steady-state overpressuring (Dickinson, 1953; Hubbert and Ruby 1959; Fertl, 1976; Neuzil, 1995). However, compaction of rocks is limited by available porosity. At typical permeability of trapping rocks ~ 10^{-20} m^2, hydraulic gradient 400 bar/km and temperature 100°C, the overpressured zone looses pore water with rate 43 m of water column per million of years (see Eq. 20). Thus, compaction of the overpressured zone with thickness 430 m by 10 % takes about 1 million of year. More detailed modeling gives lifetime for the overpressured zone about few tens of millions of years (Vejbæk, 2008). Another popular idea is based on positive volume change at the conversion of kerogen to liquid hydrocarbon (Spencer, 1987). However, this process has similar lifetime (McPherson and Bredehoeft, 2001), whereas overpressured zones are known in Cambrian deposits (Fenin, 2010). Thus, in addition to temporal factors, there should be special mechanism, which "pumps" water back into zones of abnormal pressure.

Small overpressures may be easily explained by artesian mechanism (Hubbert and Rubey, 1959; Fertl, 1976; Neuzil, 1995). If the feeding area of aquifer is located on the hills, elevated by 1000 m over valley, this gives overpressure about 100 bar (on the mouth of well, drilled in valley). However, at higher overpressures, artesian mechanism looks doubtful, like a feeding area of aquifer at the top of Himalaya Mountain (note that such hypothetical mountain should be located near each oil field). Similarly, the difference in density of water and oil or gas may give significant overpressures (Hubbert and Rubey, 1959; Fertl, 1976; Neuzil, 1995). However, at density of oil 0.8-0.9 g/cm^3, the overpressure 100 bars may be reached in fantastic 5-10 km oil column.

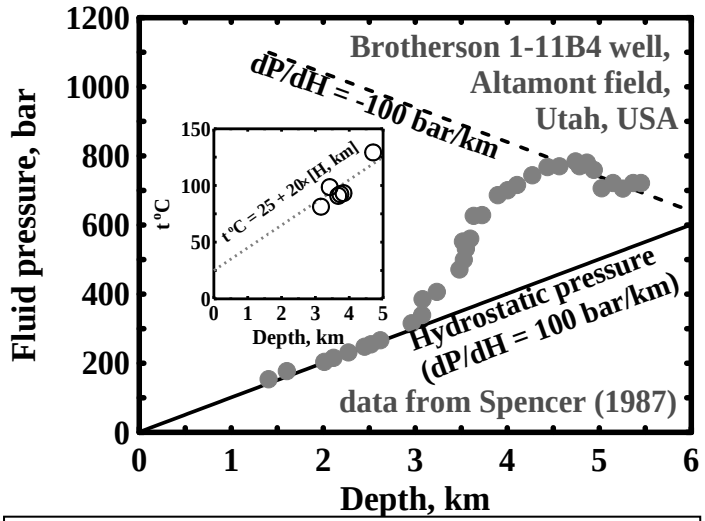

Fig. 7 Pressure profile (insert: temperature) in the Shell 1-11B4 Brotherson well (Altamont oil field, Uinta basin, Utah, USA). Data from Spencer (1987). Note negative slope below 4.7 km.

In accordance with Van't Hoff equation, pressure jump between the fresh and salt waters, separated by semi-permeable membrane, is

$$\Delta P_{osm}, \text{ bar} = -83.144\times\{T\omega/[V_w, \text{ cm}^3/\text{mol}]\}\Delta\ln(a_w) \sim 0.083144\times T\omega\nu[\Delta c, \text{ mol/L}] \quad (44)$$

Here ω is osmotic efficiency (≡ reflection coefficient, ranging from 0 to 1), a_w is activity of water (roundly, mole fraction), c is salt concentration, ν = 2 for NaCl, 3 for $CaCl_2$, etc. As one may calculate from Van't Hoff equation, the osmotic pressure of NaCl-saturated brine at 25°C (a_w = 0.753; c = 6.15 mol/kgH_2O = 5.42 mol/L) in contact with fresh water is 389 bar, if ω = 1. In some studies, this mechanism was suggested as a major factor for the generation of the abnormal pressure (Marine and Fritz, 1981; Fritz, 1986). However, osmotic efficiency of clay membranes drops to zero above c ~ 0.01 mol/L (Kemper and Rollins, 1966; Bresler, 1973), whereas osmotic pressures, measured on clay membranes, do not exceed 1 bar (Tremosa, 2010).

Some studies report surprisingly low pressures, measured just below the zone of abnormally high pressures (Spencer, 1987; Liong and Nian, 2009). As may be seen in **Fig. 7**, the pressure-depth relation may be rather mysterious: fluid pressure may decrease with depth. From data of Spencer (1987), pressure-depth gradient at depth 5 km for Altamont oil field is about of

–100 bar/km (see dashed line in **Fig. 7**). Thus, hydraulic pressure gradient in water column is –100 –100 = –200 bar/km. Thermal gradient for the Altamont field is about of ~ 20°C/km (Spencer 1987; see insert in **Fig. 7**). Thus, dP_h/dT = – 10 bar/K.

So on, one may guess, that the thermo-diffusion is an important driving force for the generation of abnormal pressure (see **Fig. 8**). Indeed, in water-saturated porous medium, water flows from hot to cold (Srivastava and Avasthi, 1975; Dirksen, 1969). This reflects tendency for evaporation in the hot zone and for condensation in the cold zone. Such tendency exists, although the porous medium is completely filled by liquid. However, maximum values of dP_h/dT, measured in experiment, do not exceed few cm of water column per °C (except value 4.2 cm Hg/°C = 57 cm H_2O/°C, measured by Srivastava and Avasthi, 1975, on "highly compressed kaolinite"). On basis of these observations, the thermo-osmotic pressure is zero, at least, in geological sense (Gray, 1966). Nevertheless, life is short, and the measurement of thermo-osmotic pressure may be performed in porous medium with relatively high hydraulic permeability. Contrarily, the Nature has much more time.

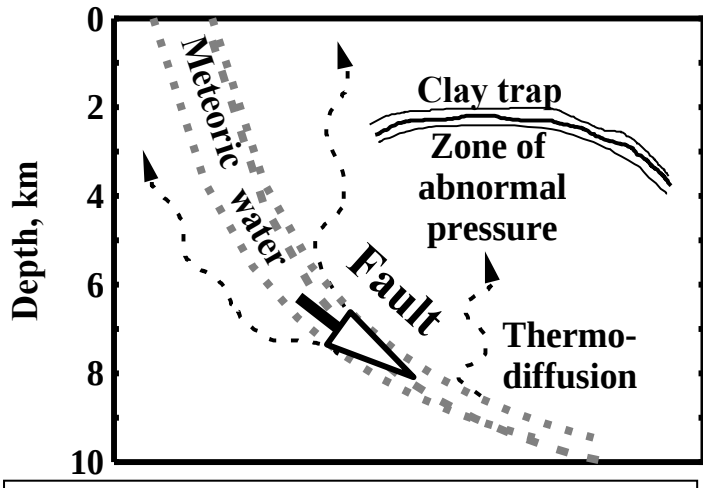

Fig. 8 Scheme of zone of abnormal pressure above the fault. Fluid pressure in the fault is hydrostatic.

SUBJECT OF PRESENT STUDY The present study is an attempt to create the theory of thermo-osmotic pressure.

HYPOTHESIS

Let us assume that Eqs. (36) is applicable (at least, approximately) in the field of thermal gradient. If this is true, Eq. (36) may be rewritten as

$$\upsilon_d\ ,\ m/s \sim - D^o \times \{\partial \ln(f)/\partial T\}_P \times \{dT/dx\} - D^o \times \{\partial \ln(f)/\partial P\}_T \times \{dP_h/dx\} \qquad (45)$$

It should be noted that Eq. (45) is not more than prognostic relation. In reality, diffuse flux may be disturbed by heat flux, which should cause cross-linked effects.

From Eq. (45), applying $\upsilon_d = 0$, one may obtain:

$$\Gamma^o \equiv \{dP_h/dT\}_{\upsilon=0,\ k=0} \sim - \{\partial \ln(f)/\partial T\}_P / \{\partial \ln(f)/\partial P\}_T \qquad (46)$$

Here Γ^o is limiting thermo-osmotic pressure at zero hydraulic permeability. In porous medium, both terms in Eq. (45) should be corrected on tortuosity. Eq (46), however, remains valid for porous medium without changes.

From general thermodynamics (Karapetyants, 1975):

$$\{\partial \ln(f)/\partial T\}_P = H_{vap}/RT^2 \qquad (47)$$

Here H_{vap} is enthalpy of vaporization into vacuum (J/mol, positive value), i.e, $\{H_{P\to 0,\ T} - H_{P,T}\}$, where $H_{P\to 0,\ T}$ is enthalpy of water vapor at given T in the limit P→0 (J/mol, negative value), and $H_{P,T}$ is enthalpy of pure water at given T, P (J/mol, very negative value).

Tab. 4 Enthalpy of vaporization of liquid water into vacuum. Sign "*" indicates supercooled liquid (in the field of ice). Bold italic style: low density gas-like state (in supercritical region).

T°C	H_{vap} , kJ/mol							
	P_{sat}	100bar	200bar	500bar	1 kbar	2 kbar	5 kbar	10kbar
0°C	44.6*	44.4	44.3	43.8	42.9	41.4	37.0	30.4*
25°C	44.0	43.8	43.7	43.2	42.4	40.9	36.5	29.9*
50°C	43.1	42.9	42.8	42.3	41.5	40.0	35.8	29.2
100°C	40.9	40.7	40.6	40.2	39.5	38.1	34.1	27.6
150°C	38.5	38.4	38.3	38.0	37.4	36.2	32.3	25.9
200°C	36.2	36.2	36.1	35.9	35.4	34.3	30.6	24.3
250°C	34.1	34.1	34.1	34.0	33.6	32.6	29.1	22.9
300°C	32.3	32.3	32.3	32.2	31.9	31.1	27.7	21.5
400°C	-	***4.6***	***11.4***	24.7	27.8	27.0	24.6	18.9
600°C	-	***0.9***	***1.4***	***6.4***	16.1	20.5	19.7	14.5

Tab. 5 Limiting thermo-osmotic pressure of liquid water, Γ^o, bar/K. All values of Γ^o are negative. Sign "*" indicates supercooled liquid (in the field of ice). Bold italic style: low density gas-like state (in supercritical region).

T°C	$-\Gamma^o$, bar/K							
	P_{sat}	100bar	200bar	500bar	1 kbar	2 kbar	5 kbar	10kbar
0°C	90.6*	90.7	90.9	91.1	91.0	90.9	87.2	77.4*
25°C	81.7	81.7	81.8	82.0	82.0	81.7	78.1	69.1*
50°C	73.1	73.1	73.3	73.3	73.3	72.9	69.9	61.5
100°C	58.3	58.3	58.5	58.7	58.8	58.7	56.4	49.3
150°C	46.3	46.4	46.6	47.0	47.4	47.6	46.0	40.0
200°C	36.7	36.9	37.1	37.7	38.4	38.9	37.9	32.8
250°C	28.9	29.1	29.5	30.4	31.3	32.1	31.7	27.4
300°C	22.4	22.5	23.0	24.2	25.5	27.6	26.7	23.0
400°C	-	***0.14***	***0.92***	11.8	15.9	17.7	19.0	16.5
600°C	-	***0.01***	***0.05***	***0.67***	3.8	7.7	10.1	8.9

Tab. 6 Critical thickness of flat channel for water (calculated from Eq. 51 and data in **Tab. 2**). Sign "*" indicates supercooled liquid (in the field of ice). Bold italic style: low density gas-like state (in supercritical region).

T°C	λ , Å							
	P_{sat}	100bar	200bar	500bar	1 kbar	2 kbar	5 kbar	10kbar
0°C	4.23*	4.22	4.21	4.18	4.14	4.07	3.92	3.78*
25°C	4.23	4.22	4.21	4.19	4.15	4.08	3.94	3.79*
50°C	4.25	4.24	4.23	4.21	4.17	4.10	3.96	3.82
100°C	4.32	4.31	4.30	4.27	4.23	4.15	4.01	3.86
150°C	4.42	4.40	4.39	4.35	4.30	4.22	4.06	3.90
200°C	4.55	4.53	4.51	4.46	4.40	4.30	4.11	3.94
250°C	4.73	4.71	4.68	4.61	4.51	4.39	4.17	3.98
300°C	5.00	4.99	4.93	4.79	4.66	4.49	4.23	4.02
400°C	-	***21.7***	***13.5***	5.55	5.07	4.74	4.37	4.11
600°C	-	***26.2***	***18.0***	***10.4***	6.94	5.51	4.70	4.30

In **Tab. 4**, the values of enthalpy of vaporization of water into vacuum H_{vap} are given. These values were calculated in accordance with Eq. 47, via numerical differentiation of data in **Tab. 1**. From Eqs. (38, 46, 47) limiting thermo osmotic pressure is

$$\Gamma^o, \text{ bar/K} \equiv \{dP_h/dT\}_{\upsilon=0,\, k=0} \sim -10^{-5}\times H_{vap}/\{V_w\times T\}$$
$$= -10^{4}\times[H_{vap}, \text{ kJ/mol}]\times[\rho_w, \text{ g/cm}^3]/\{[M_w, \text{ g/mol}]\times T\} \quad (48)$$

The values of limiting thermo-osmotic pressure, as calculated from Eq. (48), are given in **Tab. 5**. Note also that the value of Γ^o is always negative: i.e., in no-flux state, gradients of temperature and hydraulic pressure are opposite. As may be seen, this parameter decreases with temperature and almost independent of pressure up to few kbar. However, in the gas and gas-like field, Γ^o approaches to zero (see values in bold italic style).

If hydraulic flux is comparable with diffuse flux, the overall velocity of water in straight flat channel (see Eqs. 23, 45) is:

$$\upsilon \sim -\{h^2/12\eta\}\text{grad}P_h - D^o\times(\partial\ln f/\partial P)_T\times\text{grad}P_h - D^o\times(\partial\ln f/\partial T)_P\times\text{grad}T \quad (49)$$

Thus, at $\upsilon = 0$, the thermo-osmotic pressure is

$$\Gamma \equiv \{dP_h/dT\}_{\upsilon=0} \sim \Gamma^o/\{1 + (h/\lambda)^2\} \quad (50)$$

$$\lambda, \text{ m} = [12\eta D^o V_w/RT]^{0.5} = [2V_w/\pi N_A r_h]^{0.5} = \{12\tau^2\sigma\}^{0.5} =$$
$$= 4.226\times10^{-10}/[\rho, \text{ g/cm}^3]^{0.5} \quad (51)$$

Here λ is critical thickness of flat channel or fracture (see **Tab. 6**). With known parameters for 25°C and 1 bar ($\eta = 0.8904\times10^{-3}$ Pa×s; $D^o = 2.30\times10^{-9}$ m^2/s; $V = 18.07\times10^{-6}$ m^3/mol; $R = 8.3144$ J×mol^{-1}×K^{-1}), one may calculate $\lambda = 4.23$ Å. Thus, at 25°C, thermo-osmotic pressure may be calculated as (see **Tab. 5**; 1 bar = 1023 cm H_2O):

$$\Gamma, \text{ cm } H_2O/K \sim -8.36\times10^{4}/\{1+([h, Å]/4.23)^2\} \quad (52)$$

In **Fig. 9**, the data from Gray (1966) and Dirksen (1969) on thermo-osmotic pressure in water-saturated kaolinite are shown (in both studies, specific surface area of clay was not measured). Solid curves were calculated in accordance with Eq. (52), where the average distance between the particles was calculated from Eqs. (27, 28), assuming S = 3 or 10 m^2/g (as indicated near curves), and $\rho_s = 2.65$ g/cm^3. It should be noted, that the theoretical values are negative, i.e., in no-flux state, gradients of temperature and pressure are opposite. Contrarily, Gray (1966) reports positive values. He writes: "Pressure rise always occurred at the hot side". Perhaps, there is logical error. Dirksen (1969) also reports positive values, however, with opposite meaning. He writes:

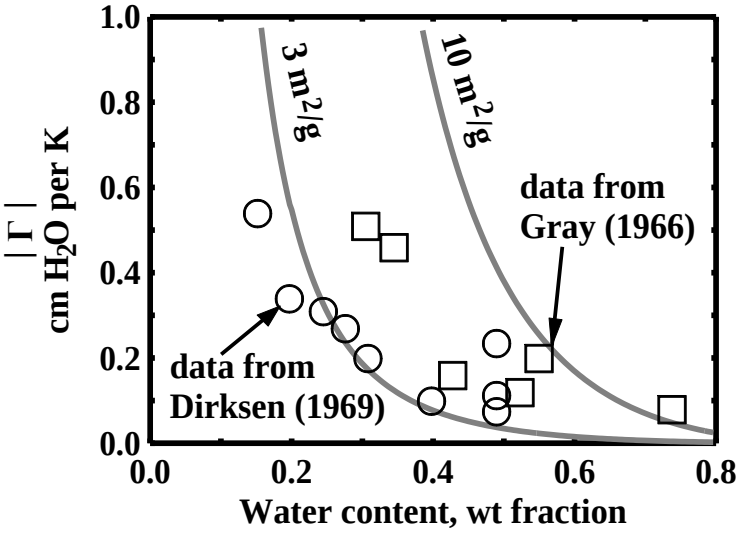

Fig. 9 Thermo-osmotic pressure (by modulus) for compacted saturated kaolinite as function of water content. Data from Gray (1966), and from Dirksen (1969). Mean temperatures 25-27°C. Fluid: water or 0.001-0.01 M NaCl solutions. Curves: Egs. (27, 28, 51) with specific surface area 3 or 10 m^2/g.

"Thermal flow occurred from warm to cold". In both cases, the specific surface area of clay samples was not measured. However, surface area ~10 m^2/g seems to be typical for kaolinites. Apart from mish-mush with sign of the effect, Eq. (52) agrees with experiment, at least, by magnitude.

Thus, Eq. (50) agrees with negligible values of thermo-osmotic pressures, measured experimentally. From the other hand, the limiting thermo-osmotic pressures (see **Tab. 5**) are rather significant in geological sense.

Fig. 10 shows fluid pressure profile, as given by Spencer (1987; the same as in **Fig. 7**). Dashed lines were drawn for thermo-osmotic pressures -2.5, -5 and -10 bar/^oC and thermal gradient 20^oC/km. In accordance with Eq. (50) and data in **Tabs. 5, 6** this corresponds to thickness of channel ~ 2, 1.4, and 1 nm (at no-flux state). From Eqs. (26, 42, 43), one may estimate permeability at ~ 16, 8 and $4\times\theta\times10^{-20}$ m^2.

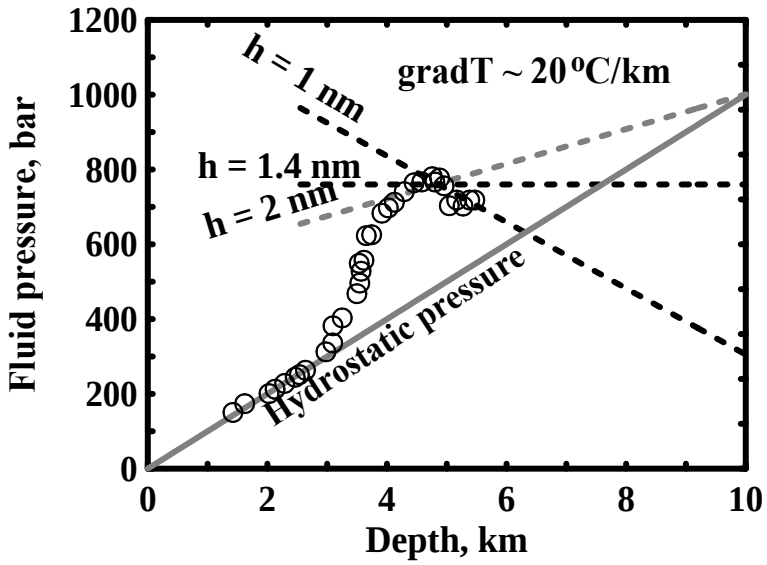

Fig. 10 Pressure profile in the Shell 1-11B4 Brotherson well (Altamont oil field, Uinta basin, Utah, USA). Data from Spencer (1987), the same as in **Fig. 7**. Dashed lines were drawn for thermo-osmotic pressures -2.5, -5, and -10 bar/^oC (at no-flux state, this corresponds to thickness of flat channel 2, 1.4 and 1 nm).

Fig. 11 shows the intrinsic permeability of "natural mudstones" in vertical direction, as measured by Yang and Aplin (2007). Each point corresponds to one of 23 samples taken from 16 wells at depths 2-5 km (clay content 12-66 %; North Sea, and Bay of Mexico). Dashed curves are $k = 4\times\theta\times10^{-20}$ and $16\times\theta\times10^{-20}$ m^2. As may be seen, typical hydraulic properties of gas-oil trap rocks are favorable for generation of significant thermo-osmotic pressures.

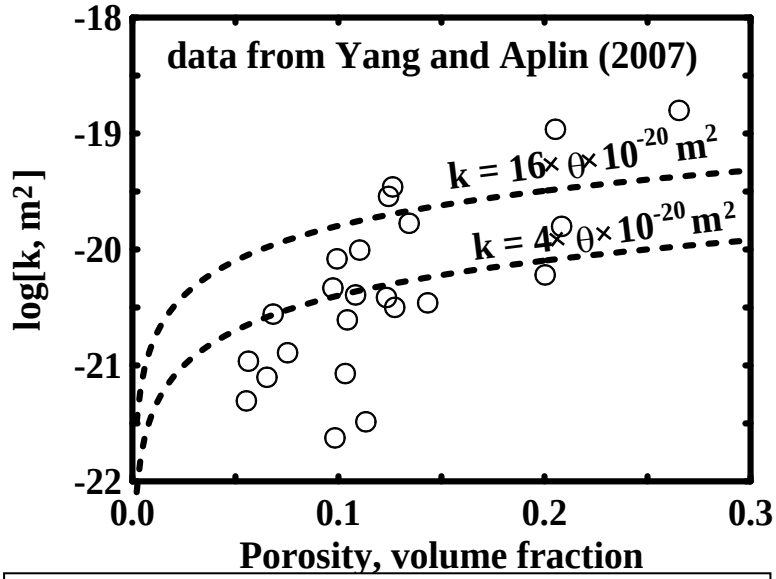

Fig. 11 Intrinsic permeability of "natural mudstones" in vertical direction (23 samples taken from 16 wells at depths 2-5 km). Data from Yang and Aplin (2007).

Thus, it is possible that thermo-osmosis is mechanism which "pumps" zones of abnormal pressure. More other, at depths 20-40 km, permeability ~ 10^{-20} m^2 is typical for crystalline rocks of the Earth's crust (Shmonov et al, 2002). Therefore, the same thermo-osmotic mechanism may be responsible for the extra dry conditions in the deep Earth.

CONCLUDING REMARKS

It is possible, that the thermal diffusion of water is important factor for the generation of abnormally high pressures. This hypothesis does not contradict with negligibly small values of thermo-osmotic pressure, measured in laboratory. Low values of thermo-osmotic pressure are affected by large hydraulic flux. Geologically significant effects may be expected, if diffuse flux accounts for, at least, few percents of total flux, i.e., at thickness of pores about several nanometers, or at permeability of rock ~ 10^{-20} m^2 and smaller. Such properties of rocks are expected to be typical below few tens of kilometers. Thus, in the deep Earth, diffuse flux of water dominates over hydrodynamic one. And it is likely, that the deep Earth is specified by extra dry conditions. This is because water is too light to compete with stones and iron for the space in the deep Earth. And, because the deep Earth is too hot to be wet.

REFERENCES

Aranovich LYa (1991) Mineral'nie ravnovesiya mnogocomponentnih tverdih rastvorov (Mineral equilibria of multicomponent solid solutions, in Russian). Moscow: "Nauka".

Beard DC and Weyl PK (1973) Influence of texture on porosity and permeability of unconsolidated sand. Amer. Assoc. Petrol. Geol. Bull. 57, 349-369.

Bresler E (1973) Anion exclusion and coupling effects in nonsteady transport through unsaturated soils: I. Theory. Soil Sci. Soc. Am. Proc. 37, 663-669.

McPherson BJOL and Bredehoeft JD (2001) Overpressures in the Uinta basin, Utah: Analysis using a three-dimensional basin evolution model. Water Resour. Res. 37, 857-871.

Carman PC (1937) Fluid flow through granular beds. Trans. Inst. Chem . Eng. 15, 150-166.

Dickinson G (1953) Geological aspects of abnormal reservoir pressures in Gulf Coast Louisiana. Amer. Assoc. Petrol. Geol Bull. 37, 410-432.

Dirksen C (1969) Thermo-osmosis though compacted saturated clay membranes. Soil Sci. Soc. Amer. J. 33, 821-826.

Djéran-Maigre I, Tessier D, Grunberger D, Velde B, Vasseur G (1998) Evolution of microstructures and of macroscopic properties of some clays during experimental compaction. Marine and Petrolum Geology 15, 109-128.

Fertl WH (1976) Abnormal formation pressures. Implications to exploration, drilling, and production of oil and gas resources. Elsevier, Amsterdam-Oxford-New York.

Gray DH (1966) Coupled flow phenomena in clay-water systems. Univ. of Michigan. Industry program of the College of Engineering. (as printed on title page; however, this document is often referred as "Ph.D. Thesis. Univ. of California, Berkley." Perhaps, there are two versions of this document.)

Grigull U, Straub J, Schiebener P (1990) Steam Tables in SI-Units, 3rd ed. Berlin: "Springer-Verlag".

Hao F, Zou H, Gong Z, Yang S, Zeng Z (2007) Hierarchies of overpressure retardation of organic matter maturation: case studies from petroleum basins in China. Amer. Assoc. Petrol. Geol. Bull. 91, 1467-1498.

Hubbert MK and Rubey WW (1959) The role of pore pressure in mechanics of overthrust faulting. Bull of Geol. Soc. of Am. 70, 115-166.

Fenin GI, Travina TA, Chumakova OV (2008) Problemi osvoeniya zalezhey s povishennimi i anomal'nimi plastovimi davleniyami. (Problems of exploration of deposits with elevated and abnormal formation pressures, in Russian). Neftegazovaya geologiya. Teoriya i praktika. 3, 9 pages, http://www.ngtp.ru/rub/4/39_2008.pdf

Fenin GI (2010) Anomal'nie plastovie davleniya v zonah uglevodorodonakopleniya neftegazonosnih basseynov (Abnormal formation pressures in zones of hydrocarbon

accumulation in oil-gas basins, in Russian). Neftegazovaya geologiya. Teoriya i praktika. 5, 20 pages, http://www.ngtp.ru/rub/4/46_2010.pdf

Fritz SJ (1986) Ideality of clay membranes in osmotic processes: a review. Clays Clay Miner. 34, 214-233.

Karapetyants MH (1975) Himicheskaya termodinamika (Chemical thermodynamics, in Russian). Moscow: "Himiya".

Kemper WD, Rollings JB (1966) Osmotic efficiency coefficients across compacted clay. Soil Sci. Soc. Am. J. 36, 426-433.

Krynicki K, Green CD, Sawyer DW (1980) Pressure and temperature dependence of self-diffusion in water. Faraday Discuss. Chem. Soc. 66,199-208.

Kutepov AM, Polyanin AD, Zapryanov ZD, Vyaz'min AB, Kazenin DA (1996) Himicheskaya gidrodinamika: spravochnoe posobie (Chemical hydrodynamics: hand-book, in Russian) Moscow: "Byuro Kvantum".

Leftwich JT Jr and Engelder T (1994) The characteristics of geopressure profiles in the Gulf of Mexico basin. In: Basin compartment and seals (Ed.: Ortoleva PJ). Amer. Assoc. Petrol. Geol. Mem. 61, 119-129.

Luong TV, Nan NH (2009) Osobennosti raspredeleniya i izmeneniya plastovih davleniy v granitoidnih kollectorah mestorozhdeniya "Beliy tigr" (Peculiarities of distribution and changes of formation pressures in granitoid collectors of deposit "White tiger", in Russian). Neftegazovoe delo 2009, 9 pages, http://ogbus.ru/authors/Luong/Luong_1.pdf

Marine IW, Fritz SJ (1981) Osmotic model to explain anomalous hydraulic heads. Water Resources Res. 17, 73-82.

Neuzil CE (1995) Abnormal pressures as hydrodynamic phenomena. Amer. J. of Sci. 295, 742-786.

Pivovarov S (2013) Simple equation of state for water, carbon dioxide, metane, and their mixtures. Basis 1, 1-12, http://basisj.narod.ru/Basis2013_1-12.pdf

Shmonov VM, Vitovtova VM, Zharikov AV (2002) Fluidnaya pronitsaemost' porod zemnoy kori (Fluid conductivity of rocks of Earth's crust, in Russian). Moscow: "Nauchniy mir", 216 pages.

Spencer ChW (1987) Hydrocarbon generation as a mechanism for overpressuring in Rocky Mountain Region. Amer. Assoc. Petrol. Geol. Bull. 71, 368-388.

Srivastava RC, Avasthi PK (1975) Non-equilibrium thermodynamics of thermo-osmosis of water through kaolinite. J Hydrol. 24, 111-120.

Trémosa J (2010) Influence of osmotic processes on the excess-hydraulic head measured in the Toarcian/Domerian argillaceous formation of Tournemire. Thesis, Univ. Pierre and Marie Curie.

Vejbæk OV (2008) Disequilibrium compaction as the cause for Cretaceous-Paleogene overpressures in the Danish North Sea. Amer. Assoc. Petrol. Geol. Bull. 92, 165-180.

Yardley BWD, Valley JW (1997) The petrologic case for a dry lower crust. J. Geophys. Res. 102, 12173-12185.

Yang Y, Aplin AC (2007) Permeability and petrophysical properties of 30 natural mudstones. J Geophys. Res. 112, 14 pages.